ELSEVIER

Novel honeycombs with auxetic behaviour

N. Gaspar [a,*], X.J. Ren [b], C.W. Smith [a], J.N. Grima [c], K.E. Evans [a]

[a] *School of Engineering, Computer Science and Mathematics, University of Exeter, North Park Road, Exeter, EX4 4QF, UK*
[b] *School of Engineering, Liverpool John Moores University, Liverpool L3 3AF, UK*
[c] *Department of Chemistry, Faculty of Science, University of Malta, Msida MSD 06, Malta*

Abstract

Materials with a negative Poisson's ratio have been modelled largely by regular 2D networks. These models represent the conceptual features of the microscale of materials with a negative Poisson's ratio. To date they do not reflect the detail or exact structure of any known auxetic material. In this paper, 2D materials have been constructed whose microstructure is represented exactly by the auxetic models. These materials are subjected to an axial strain and the measured Poisson's ratio is compared to the predictions by the models. The models are also amended to fit better the observed deformation within the 2D materials. The models are found to predict some behaviour reasonably well but only when model parameters are measured from the experimental data.
© 2005 Acta Materialia Inc. Published by Elsevier Ltd. All rights reserved.

1. Introduction

A variety of materials with negative Poisson's ratios, and their advantages over conventional positive ratio materials, have been investigated (Lakes [1,2], Alderson et al. [3], Grima et al. [4], Alderson and Evans [5], Smith et al. [6], Gaspar et al. [7]). For a review, see Alderson and Evans [8]. Most of these materials have a microstructure that induces a negative Poisson's ratio at a macroscale. For instance the microstructure of an auxetic foam is the three-dimensional array of discrete ribs. These ribs interact together so that a statistically large sample (macroscale) displays a negative Poisson's ratio. Other examples are molecular auxetics, in particular zeolite. Here, the microstructure is the organisation of molecules into a crystal (macroscale). Through molecular modelling these crystals are predicted to display a negative Poisson's ratio.

Importantly there are a wide variety of auxetic materials, and although many features may be similar from one material to another, in general the microstructures also vary widely. This variation can be observed in terms of geometry (the ribs of an auxetic foam do not visually resemble the atomic structure of zeolite), but also in terms of length scale. Molecular auxetics are the smallest with a microstructure length scale of the order of nanometres. The largest microstructure known to date is the nuclear reactor core with a length scale of tens of metres Several investigators have proposed various network-like structures as potential microstructures for the generation of auxetic behaviour. These structures can be used to model existing auxetic materials such as foams, or used to describe potential materials such as molecular auxetics.

Some of these networks allow for more than one deformation mechanism to take place concurrently within the microstructure (Alderson et al. [3]). Usually, concurrent deformation is assumed to be negligible, in part because in some cases there is little experimental evidence for it (Smith et al. [6]), because measurement

---

* Corresponding author. Tel.: +44 1483 564551; fax: +44 1483 262626.
E-mail address: n.gaspar@physics.org (N. Gaspar).

of internal deformation has been difficult, and also in part because of the simplification attained in calculations.

A material has been made from a regular plastic mesh with a microstructure that exactly matches the theoretical model by Smith et al. [6]. This work records experiments that measure the macroscopic variables of Poisson's ratio and strain and also microscopic variables of the geometry of the microstructure. In this way, real experimental values of the Poisson's ratio can be obtained to compare with the model's values, and also the deformation mechanisms of the microscale can be observed.

2. Materials and testing methods

The period of the mesh used was about 10 mm, although as is highlighted in the introduction, it is the geometry of the microscale not its absolute length that is of primary interest. In all, four different 2D samples were constructed: samples 1 and 2 used the mesh in its original state with the microstructure orientated parallel and obliquely to the sample axis, respectively; samples 3 and 4 had selected ribs removed to emulate two versions of the model by Smith et al. [6] with the intention of creating a network with a negative Poisson's ratio. The microstructures of the samples are shown in Fig. 1.

The testing procedure is schematically shown in Fig. 2. The meshes were clamped at both ends and subjected to a strain along one axis, three pairs of markers were used in both longitudinal and lateral directions, located approximately at $\frac{1}{4}$, $\frac{1}{2}$ and $\frac{3}{4}$ of the length and width. The mesh under strain was imaged and digitised. The change of the separation between the markers in the two directions (longitudinal and lateral) were measured from the digitised images and the axial strains were calculated as follows:

$$\epsilon_x = \frac{x_n - x_0}{x_0}, \tag{1}$$
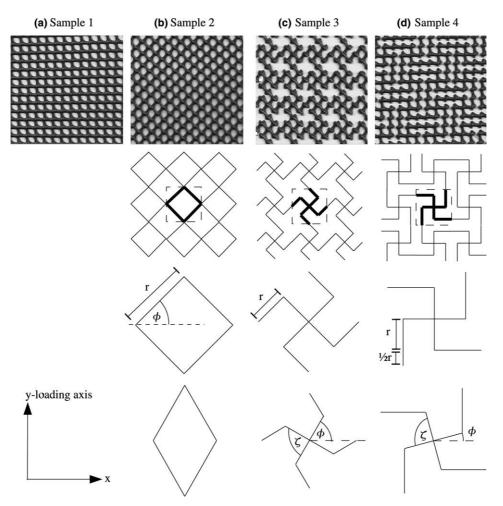
$$\epsilon_y = \frac{y_n - y_0}{y_0}, \tag{2}$$

Fig. 1. Details of the conventional and missing rib foams. Samples 1–2: conventional; samples 3–4: auxetic. Row 1: image of microstructure. Row 2: tessellation of modelled unit cell. Row 3: undeformed, modelled unit cell. Row 4: deformed, modelled unit cell.
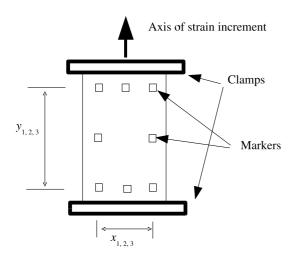
Fig. 2. Schematic show of the testing methods.

Fig. 3. Measured Poisson's ratio as a function of strain.

where x_n is the separation between markers at then nth step of loading, x_0 and y_0 are the original separations between the markers. The average strain for the materials was calculated by taking the average of the strain determined from the three pairs of markers. Then the Poisson's ratio is calculated from the average strains by

$$v_{yx} = -\frac{\langle \epsilon_y \rangle}{\langle \epsilon_x \rangle}. \qquad (3)$$

3. Macroscopic experimental results

3.1. Experimental error

The principal experimental error is in measuring the location of the markers from the digitised images. A sensible estimate is that there is an uncertainty of ±4 pixels in the measurement of a length from the digitised images. When calculating a strain, this uncertainty corresponds to the magnitude of the strain measured at the first and sometimes second data points in an experiment. This should be recognised when making conclusions on the strain behaviour of the sample. The Poisson's ratio calculated from these points will also be subject to error. Due to the denominator approaching zero, the experimental error can cause the Poisson's ratio at low strain to be wildly inaccurate. For this reason, it is worth discounting data points of strain and Poisson's ratio where the vertical strain is less than 1%.

3.2. Poisson's ratio vs. strain

The Poisson's ratio as calculated by Eq. (3) is plotted against the engineering strain in Fig. 3. Samples 1 and 2 exhibit a positive Poisson's ratio. The strain-dependent behaviour of sample 1 is hard to ascertain from the available data due its narrow strain range. However, sample 2 shows a steady increase to about $v = 0.85$.
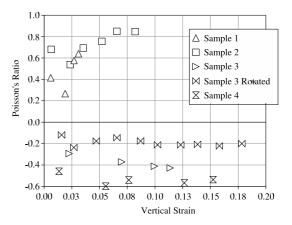
Samples 3, 3 rotated, and 4 behave quite differently. All three experiments demonstrate a negative Poisson's ratio and, unlike sample 2, the Poisson's ratio does not change rapidly with strain. This is similar to the predictions by Smith et al. [6].

The models given by Smith et al. [6] use microscopic information about the mesh such as internal angles and rib length, to predict strains and Poisson's ratio. So to examine the relationship between the models and these experimental results, microscopic data from the networks must be obtained.

4. Microscopic experimental results

The microstructure of the materials, as shown in Fig. 1, and used by Smith et al., is assumed to consist of ribs that meet at joints, the angle of which can deform elastically, and that the ribs are arranged in cells that have translational symmetry. At each strain point to which the samples were subjected, a digital image was taken. From these images the microstructural parameters were measured at each strain point. That is, the angle and length of each rib was measured for each of 20 unit cells.

The rib lengths were found to change very little. For example in sample 2, the mean rib length changed by 0.6% across the total strain path. This can be compared to the global mean strain and also to the variation of rib length at a single strain point. In the former case, the mean change of rib length is much smaller than the 8.2% mean global strain. In the latter case, the change of rib length is again smaller than the 2.4% normalised standard deviation of the spread of rib lengths measured at the final strain point. Note that the normalised standard deviation is taken as the standard deviation of the sample of values divided by mean of the values. In essence, the ribs are considered to remain almost unchanged in length and so the only constitutive parameters considered any further are internal angles identified in Fig. 1 and recorded in Table 1.

Table 1
Mean values of angles. TC is the total change in the value between the initial and the final strain point and the standard deviation (SD) is taken at the final strain point over 20 cells

Sample	Angle	Angle data point											TC	SD
		0	1	2	3	4	5	6	7	8	9	10		
2	ϕ	43.0	43.5	44.5	45.1	46.1	47.2	47.8					4.8	1.1
3	ζ	91.8	93.1	94.0	96.1	97.0							5.1	2.3
	ϕ	48.5	50.8	52.4	56.1	56.2							7.7	2.7
3	ζ	88.7	88.6	66.3	88.6	88.7	89.5	90.6	91.3	91.6	92.6	92.9	4.1	1.8
90°	ϕ	44.5	44.5	45.4	45.9	47.2	49.4	48.7	52.0	52.0	54.3	53.7	9.2	1.0
4	ζ	91.2	91.4	92.9	93.1	94.6	96.8						5.6	6.1
	ϕ	0.4	5.4	10.0	12.1	17.3	21.3						21.0	4.5

5. Analytical models

In Smith et al. [6], a theoretical model is reported that gives the Young's modulus and Poisson's function for 2D honeycombs that correspond with samples 2 and 3 but not 4. A similar procedure is applied below to obtain the Poisson's ratio for sample 4. The principal assumptions for the deformation are: (a) the angles between ribs deform elastically; (b) no change of length of the individual ribs is allowed; (c) the translational symmetry of the unit cell is kept throughout deformation.

The elastic angular deformation is defined by $m_A = k_A dA$ $(A = \phi, \zeta)$, where m_A is the force moment about a rib, dA is the increment of angle of the rib and k_A is the linear spring constant. Their model also requires the central spring constant to be much greater than the outer ones $(k_\zeta \gg k_\phi)$ to prevent the central spring from flexing and make negligible the effect of concurrent deformation. For this work here, flexing of the spring is included by writing the change of angle ζ as a fraction κ, of the change of angle ϕ. Hence

$$\Delta\zeta = \kappa\Delta\phi, \quad \text{where } \Delta\zeta = \zeta_n - \zeta_0, \text{ etc.} \tag{4}$$

All references to angle ζ can then be written in terms of the angle ϕ by

$$\zeta_n = \zeta_0 + \kappa\Delta\phi. \tag{5}$$

5.1. Model for sample 2 (Smith et al. [6])

Engineering strain:

$$\epsilon_x = -2r\left(\frac{\cos\phi_n}{\cos\phi_0} - 1\right), \tag{6}$$

$$\epsilon_x = -2r\left(\frac{\sin\phi_n}{\sin\phi_0} - 1\right). \tag{7}$$

Poisson's ratio:

$$v_{yx}^{\text{ratio}} = -\tan(\phi_0)\frac{\cos\phi_n - \cos\phi_0}{\sin\phi_n - \sin\phi_0}. \tag{8}$$

5.2. Model for sample 3 (Smith et al. [6])

Engineering strain:

$$\epsilon_x = 4r\left(\frac{\cos(\zeta_0 - \phi_0 + \Delta\phi(\kappa - 1))}{\cos(\zeta_0 - \phi_0)} - 1\right), \tag{9}$$

$$\epsilon_y = 4r\left(\frac{\sin\phi_n}{\sin\phi_n} - 1\right), \tag{10}$$

where $\kappa = \Delta\zeta/\Delta\phi$ is a measure of the relative deformation between the ζ and ϕ springs. Setting $\kappa = 0$ restores the assumption of no concurrent deformation. Poisson's ratio at strain point n

$$v_{yx}^{\text{ratio}} = -\frac{(\cos(\zeta_0 + \phi_0 + \Delta\phi(\kappa - 1)) - \cos(\zeta_0 - \phi_0))\sin\phi_0}{(\sin\phi_n - \sin\phi_0)\cos(\zeta_0 - \phi_0)}. \tag{11}$$

5.3. Model for sample 4

The microstructure for sample 4 is shown in Fig. 1. The physical size of the unit cell is given by:

$$x = 2r\left(\tfrac{3}{2} + \cos(\zeta - \phi)\right), \tag{12}$$

$$y = 2r\left(\tfrac{3}{2} + \sin\phi\right). \tag{13}$$

Using $E_x = (x_n - x_0)/x_0$ for the engineering strain along the x-axis, and equivalent for the engineering strain along the y-axis, the Poisson's ratio is

$$v_{yx}^{\text{ratio}} = \frac{(\cos(\zeta_0 - \phi_0 + \Delta\phi(\kappa - 1)) - \cos(\zeta_0 - \phi_0))\left(\tfrac{3}{2} + \sin\phi_0\right)}{(\sin(\phi_0 + \Delta\phi) - \sin\phi_0)\left(\tfrac{3}{2} + \cos(\zeta_0 - \phi_0)\right)}. \tag{14}$$

6. Model and experimental analysis

The values of the microscale variables, ζ and ϕ are listed in Table 1 and plotted in Fig. 4. The parameter
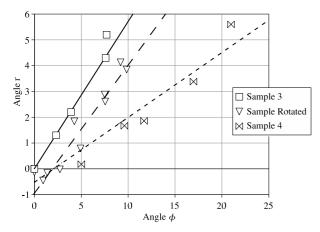
Fig. 4. Fitting model k parameter to samples 3 (square symbol, solid line), 3 rotated by 90° (triangular symbol, dashed line) and sample 4 (bow–tie symbol dotted line). The lines are fitted to the experimental data to give $k = 0.57, 0.50, 0.25$ for samples 3, 3 rotated by 90° and 4, respectively.

Fig. 6. Measured and modelled Poisson's ratio as a function of constitutive angle ϕ for sample 2.

$\kappa = \Delta\zeta/\Delta\phi$ is obtained from the gradients of lines of best-fit. The models for engineering strain and Poisson's ratio can be calculated using these measured values of κ, ζ and ϕ and are plotted in Figs. 5–12. Where the models are also plotted for $\kappa = 0$, a material that does not have concurrent deformation is being described.

6.1. Sample 2

In Figs. 5 and 6, the vertical strain is well predicted but the horizontal strain is over predicted by a constant amount of 0.015. This over prediction could be caused by a settling of the sample in the initial stages of the test. As a result the Poisson's ratio is better predicted at higher strains.

Fig. 7. Measured and modelled engineering strain as a function of angle ϕ for sample 3. Solid line and bow–tie symbol are vertical strain, dashed line and triangles are horizontal strain.
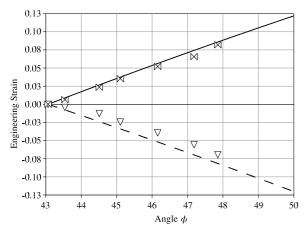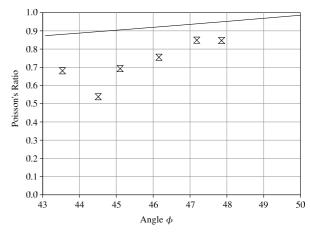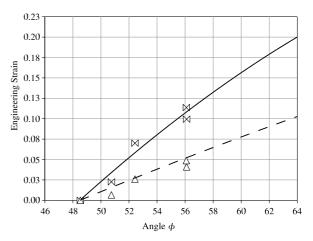

Fig. 5. Measured and modelled engineering strain as a function of angle ϕ for sample 2. Solid line and bow–tie symbol are vertical strain, dashed line and triangles are horizontal strain.
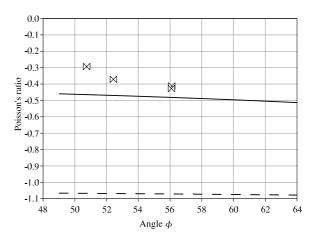

Fig. 8. Measured and modelled Poisson's ratio as a function of constitutive angle ϕ for sample 3. Solid line indicates $\kappa = 0.57$ and dashed line indicates $\kappa = 0.00$.
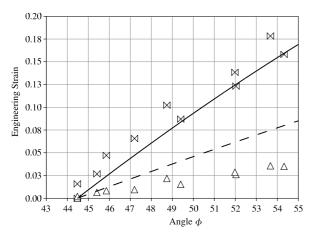
Fig. 9. Measured and modelled engineering strain as a function of angle ϕ for sample 3 rotated 90°. Solid line and bow–tie symbol are vertical strain, dashed line and triangles are horizontal strain.
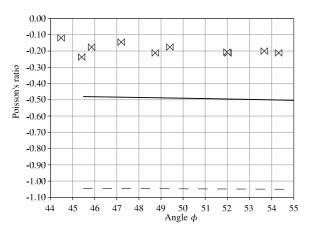

Fig. 10. Measured and modelled Poisson's ratio as a function of constitutive angle ϕ for sample 3 rotated 90°. Solid line indicates $\kappa = 0.50$ and dashed line indicates $\kappa = 0.00$.
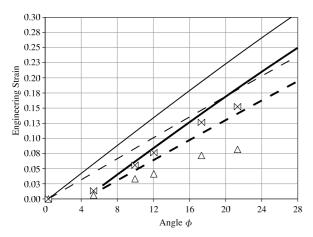

Fig. 11. Measured and modelled engineering strain as a function of angle ϕ for sample 4. Solid line and bow–tie symbol are vertical strain, dashed line and triangles are horizontal strain. Thick lines are models with adjusted start point.
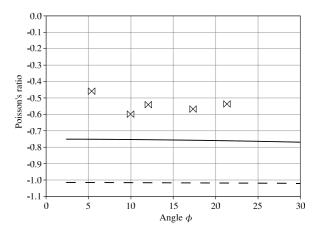

Fig. 12. Measured and modelled Poisson's ratio as a function of angle ϕ for sample 4. Solid line indicates $\kappa = 0.25$ and dashed line indicates $\kappa = 0.00$.

6.2. Sample 3

Fig. 4 gives $\kappa = 0.57$ to be used in this model. The model is seen in Fig. 7 to over predict the magnitude of the Poisson's ratio by 0.15–0.05. If κ is taken to be zero, the model predicts a near constant value of $v = -1.1$, more than twice the measured values and the model values for $\kappa = 0.57$.

6.3. Sample 3 with 90° rotation

A mean value for the relationship between ϕ and ζ is $\kappa = 0.50$, which is taken from Fig. 4. This is used in Figs. 9 and 10. The vertical strain is well predicted but the horizontal strain is over predicted by a factor of 2.5 across the values of ϕ. This is also the factor by which the Poisson's ratio is over predicted. Setting $\kappa = 0.00$ again more than doubles the predicted value of the Poisson's ratio.

6.4. Sample 4

For this sample the value for κ from Fig. 4 is $\kappa = 0.25$. The measured graph of vertical engineering strain against angle ϕ shows the first strain step does not follow the trend of subsequent strain steps. This suggests that a material settling is happening and so the model is plotted for a strain path starting at point 1 which is for $\phi = 5.4°$ as well as a strain path starting at point zero. Whichever starting point is used for the model, the results are similar to the previous samples. The vertical strain is well predicted, the horizontal strain is over predicted and the Poisson's ratio is also over predicted. In fact the model prediction of the Poisson's ratio does not significantly change for different starting points. If, however, κ is taken to be zero, the predicted value of the Poisson's ratio increases in magnitude by 20–25% of the Poisson's ratio with a measured value of κ.

7. Discussion/conclusions

Many models of deformation within network materials make use of the assumption that there is a single mode of deformation that dominates over other modes. Some of these network models have been put forward to resemble materials that may exhibit a negative Poisson's ratio but have yet to be manufactured. The broken-rib model by Smith et al. is one such model. The results here show that a material with this microstructure does produce a negative Poisson's ratio.

The results of the work presented here also show that using concurrent deformation greatly increases the accuracy of network models. Specifically, in samples 3, 3 rotated by 90° and 4, a second elastic spring (ζ) reduces the magnitude of the Poisson's ratio predicted by network models. This reduction causes the models predicted Poisson's ratio to approach the values measured from materials specifically manufactured to resemble the models. Unfortunately, the parameter κ that is a measure of the relative balance of the two deformation modes is not readily obtainable from first principles. It is only arrived at, in this case, through experimental observation.

Two further issues arise. Firstly, the network models, still do not exactly match the measured materials for Poisson's ratio or engineering strain. It maybe that there are other deformation modes not considered. Change of length of ribs is ruled out by the results, but another possibility is bending of ribs along their length. Secondly, some 20 unit cells are used in the measurement of microscopic data. The models assume that the unit cells deform homogeneously. It is eminently possible that each unit cell varies from its neighbour, thus, changing the measured value of the Poisson's ratio. Work by Gaspar et al. [7] shows that these variations, or heterogeneity, will only work to reduce the magnitude of the Poisson's ratio. In every case, the magnitude of the Poisson's ratio is over-predicted so heterogeneity could well be important.

References

[1] Lakes R. Science 1987;235(4792):1038–80.
[2] Lakes RS, Elms K. J Compos Mater 1993;27(12):1193–202.
[3] Alderson KL, Alderson A, Evans KE. J Strain Anal Eng Div 1997;32:201.
[4] Grima JN, Evans KE. J Mater Sci Lett 2000;19(17):1563–5.
[5] Alderson A, Evans KE. Phys Chem Miner 2001;28(10):711–8.
[6] Smith CW, Grima JN, Evans KE. Acta Mater 2000;48:4349–56.
[7] Gaspar N, Smith CW, Evans KE. J Appl Phys 2003;94(9):6143–9.
[8] Evans KE, Alderson A. Adv Mater 2000;12(9):617–28.